

Correlations between two vortices in dry active matter

Felipe P. S. Júnior* and F. Q. Potiguar

*Universidade Federal do Pará, Faculdade de Física, ICEN,
Av. Augusto Correa, 1, Guamá, 66075-110, Belém, Pará, Brazil*

Jorge L. C. Domingos and W. P. Ferreira

*Departamento de Física, Universidade Federal do Ceará,
Caixa Postal 6030, Campus do Pici,
60455-760 Fortaleza, Ceará, Brazil*

(Dated: April 30, 2024)

Abstract

It was recently shown that wet active matter may form synchronized rotating vortices in a square lattice, similar to an antiferromagnetic Ising model (by considering rotation direction as spin projections). In this letter, we investigate whether such a correlated state occurs for a model of dry active matter. We achieve that by numerically simulating the dynamics of a system of active particles in the presence of two identical circular obstacles. Then, we measure the rotation velocity correlation function of both vortices as a function of the obstacle diameter, their shortest separation, called gap, and the particle density. We find that, like the observations of vortex formation in wet active matter, both vortices can synchronize their rotations in either opposite or in the same direction; we call such regimes as antiferromagnetic and ferromagnetic, respectively. We show that, for the antiferromagnetic case, both vortices keep their motion correlated by exchanging particles through the region in between them, analogously to synchronized cogs; on the other hand, for the ferromagnetic regime, both vortices merge in a single rotating cluster, similar to a belt strapped around the obstacles. Additionally, we observe the emergence of uncorrelated states at the transition between correlated states, in which only a single vortex is present, or in the large gap regime, in which the vortices are nearly independent on each other.

Keywords: Active matter, vortices, synchronization, computer simulation

I. INTRODUCTION

In active matter, particles generate their motion either by consuming their internal energy or by extracting the energy from the environment[1–4]. Active systems exhibit a complex set of nonequilibrium phenomena with a wide range of possible applicability, in which the majority is still not understood. We usually describe a collection of active particles in terms of two distinct models: dry models, in which particles do not move under the influence of hydrodynamic interactions; and wet models, in which hydrodynamic interactions are present[1]. Dry models can still be divided according to the particle-particle interaction, which can be either flocking, *e.g.*, Vicsek model [5], or Angular Brownian Motion (ABM) [6], which has a close relationship to Run-and-Tumble Dynamics (RTD) [7].

* felipe.junior@icen.br

Among several interesting properties of active systems, we can highlight the tendency to aggregate either spontaneously, where in free space the system exhibits spontaneous phase separation [6], or around rigid surfaces [8–14]; in the latter, it was shown that the aggregation process depends strongly on the local curvature [9]. Correlated to this property, there is the possibility of an active aggregate around a circular obstacle to rotate, forming the so-called active vortex, even in the absence of an external drive. Such a possibility was shown in ref [15]. Later, Mokhtari *et al.* [11] described a particle capture-and-release mechanism through which a vortex may persist for extended periods; Pan *et al.* [8] performed a deeper investigation of the dynamics of a single vortex and observed that the obstacle diameter is a key parameter that controls the dynamical regime, *i.e.*, non-existent, unstable, or stable of the vortex state. Finally, B. Qian *et al.* [13] reported on some apparent rotation of a large aggregation of self propelled particles around lattices of tiny obstacles.

On the other hand, for wet models, there is a richer literature addressing such a vortex formation, either experimentally [12, 16, 17] or numerically [17, 18]. The vortices are a consequence of mesoscale turbulence, in which the underlying fluid, perturbed by the active particles, drive them in a vortex-like pattern. In particular, in a regular square lattice of circular obstacles [19], H. Reinken *et al.* observed correlated motion in neighboring vortices formed in the center of the unit cells in which a pair of vortices can rotate, with one moving in the counterclockwise and the other in the clockwise directions indicating an antiferromagnetic ordering (the vortex rotation direction is associated with the direction of $1/2$ -spins in the Ising model). Alternatively, they can both rotate in the same direction, indicating a ferromagnetic ordering. Finally, investigations of vortex interactions are also performed in wet models, for polar, active filaments [20] and regular particles in free space [21, 22], through solutions of the Toner-Tu equation [23], and they find a variety of dynamical phases, ordered and disordered, along with coarsening of the vortices. However, studies of vortex interactions in dry active models is still lacking.

In this work, we consider a dry model for active particles to investigate the correlation (synchronization) between vortices in a pair of circular obstacles as a function of the obstacles' diameter, particle density, and the shortest distance between the obstacles (gap). We do not consider any external drive. We observe both antiferromagnetic and ferromagnetic states, whose transition can be induced based on the gap and the diameter of the obstacles. In the language of turbulence, the antiferromagnetic state corresponds to two

counter-rotating vortices, while the ferromagnetic one, to two co-rotating vortices. We also characterize both correlated and uncorrelated states through the vertical particle current horizontal profiles, *i.e.*, profiles as function of the horizontal coordinate x , and we find that uncorrelated states appear at the transition between regimes or for large gaps.

This manuscript is organized as follows: our model system is presented in Sec. II; the numerical results and discussions are presented in Sec. III and our conclusions are given in Sec. IV .

II. MODEL

We consider a two dimensional ABM [6, 24] model, composed of N soft disks of diameter σ , and an intrinsic velocity v_0 (self-propulsion). They are placed in a square box of size L , in which two identical circular obstacles (disks) of diameter D are fixed at positions $(L/2 \pm (\delta + D)/2, L/2)$, where, the gap δ is the shortest distance between them (see Fig. 1).

The disks interact through a linear spring force law $\mathbf{F}_{ij} = \kappa(d_{ij} - r_{ij})\hat{\mathbf{r}}_{ij}$ for $d_{ij} > r_{ij}$, $\mathbf{F}_{ij} = 0$ otherwise, where $r_{ij} = |\mathbf{r}_i - \mathbf{r}_j|$ is distance between particles i and j , κ is the spring stiffness, and $d_{ij} = \sigma$; for the disk-obstacle interaction, we use the same force law, but with $d_{ij} = \frac{1}{2}(\sigma + D)$ and stiffness $\kappa_{obs} = 200\kappa$ in order to approach the rigid body limit.

The dynamics of the i -th particle is given by the coupled Langevin equations

$$\mathbf{v}_i = \frac{d\mathbf{r}_i}{dt} = \mu\mathbf{F}_i + \mathbf{v}_i^f + \mathbf{A}_i(t), \quad (1)$$

and

$$\frac{d\theta_i}{dt} = \eta_i(t), \quad (2)$$

where $\mathbf{v}_i = \frac{d\mathbf{r}_i}{dt}$ is the i -th particle velocity, μ is the motility, $\mathbf{F}_i = \sum_j \mathbf{F}_{ij}$, where the sum runs over all particles and obstacles, is the total force in the i -th particle, $\mathbf{v}_i^f = v_0(\cos\theta_i(t)\hat{\mathbf{x}} + \sin\theta_i(t)\hat{\mathbf{y}})$, is the intrinsic velocity with magnitude v_0 , $\theta_i(t)$ is a Gaussian random variable $\eta_i(t)$ with magnitude η_θ that follows the usual correlation and mean values, as follows

$$\langle \eta_j(t_2)\eta_i(t_1) \rangle = 2\eta_\theta\delta(t_2 - t_1)\delta_{ij}, \quad (3)$$

$$\langle \eta_i(t) \rangle = 0. \quad (4)$$

$\mathbf{A}_i(t)$ is also a Gaussian white noise variable with intensity ξ that follows

$$\langle A_{\alpha j}(t_2)A_{\beta i}(t_1) \rangle = 2\xi\delta(t_2 - t_1)\delta_{ij}\delta_{\alpha\beta}, \quad (5)$$

$$\langle \mathbf{A}_i(t) \rangle = 0, \quad (6)$$

where, α and $\beta = x, y$. Given that our model is athermal, we set $\xi = 0$. The brackets denote, anywhere in the text, averages taken over time and distinct realizations.

We used periodic boundary conditions (PBC) in both directions. The values of the model parameters are $\sigma = 1.0$ as the length unit, $\mu = 1.0$, $L = 120$, $\kappa = 50.0$, $\kappa_{obs} = 20\kappa$, $v_0 = 1$ (which also sets the time unit), and $\eta_\theta = 0.001$ and $\phi = \frac{N\pi\sigma^2}{4(L^2 - \pi(D^2)/2)}$ as the particle density.

We calculate the angular velocity of vortex Γ_k around obstacle k on position \mathbf{R}_k , $k = l, r$ for left and right obstacles, respectively, as

$$\omega_k = \left\langle \sum_{i \in \Gamma_k} \frac{1}{N_k} \frac{\mathbf{v}_i \cdot \hat{\boldsymbol{\psi}}_{ik}}{R_{ik}} \right\rangle, \quad (7)$$

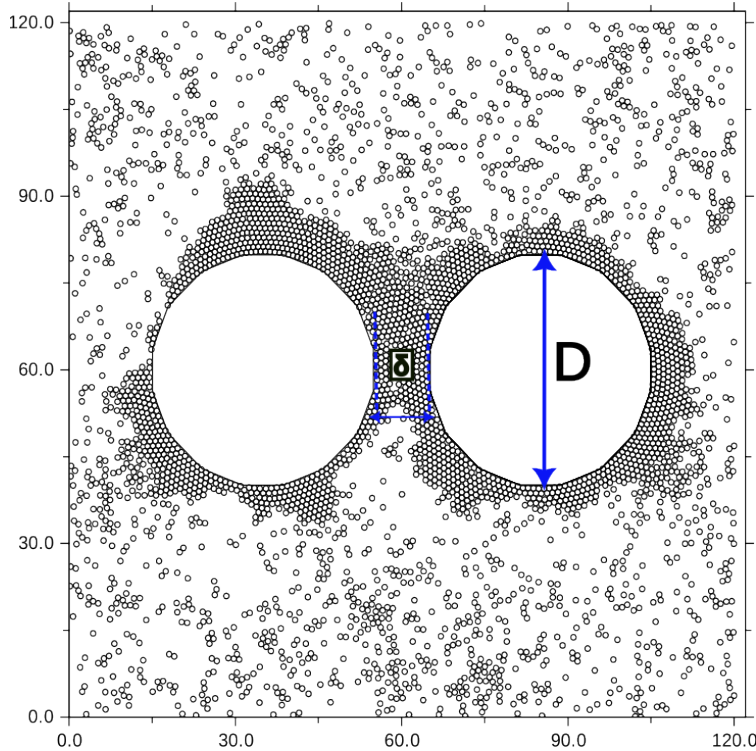


FIG. 1: Typical particle configuration for our two obstacle system of diameter D and gap δ .

where $i \in \Gamma_k$ indicates that the sum runs over the particles i that compose the vortex Γ_k around the obstacle k , $R_{ik} = |\mathbf{r}_i - \mathbf{R}_k|$, N_k the number of particles in vortex Γ_k , which

we calculate with an appropriate algorithm [25], and $\hat{\psi}_{ik}$ is the unit vector along the polar direction, as measured with the origin at the center of obstacle k . Using the angular velocities of both obstacles, we can define a global parameter, namely, the rotation velocity correlation function

$$C_{\omega_l\omega_r} = \langle \omega_l(t)\omega_r(t) \rangle, \quad (8)$$

which is a measure of the correlation between the rotational motions of each vortex.

In our simulations, we considered $\delta = [2, \dots, 20]$ with $\Delta\delta = 2.0$ and $D = [25, \dots, 40]$ with $\Delta D = 5.0$. Our numerical investigation are carried out for area fraction $\phi = [0.2; 0.25; 0.3]$, avoiding phase-separated states that appear for $\phi \geq 0.4$ [6]. We performed our measurements over 30 independent realizations of the initial conditions. In each realization, the total number of time steps is 2×10^6 with integration time step $h = 10^{-3}$.

III. RESULTS AND DISCUSSIONS

We start by presenting the general features of the correlation function that will allow us to introduce our terminology. In Figs. 2(a) and (b), we show, in the upper panels, the angular velocities of each vortex as a function of time, and in the corresponding lower panels, we show the correlation function. In Fig. 2(a), $C_{\omega_l\omega_r} = \langle C_{\omega_l\omega_r}(t) \rangle_t < 0$ indicates that the vortices rotate in opposite directions. We also observe that the magnitude of angular velocities are equivalent. Using the same analogy as in [19], we associate positive/negative rotations with up/down spins, and we call such a state as antiferromagnetic. In Fig. 3(a), we show a typical velocity field of that state. Conversely, in Fig. 2(b), $C_{\omega_l\omega_r} > 0$ indicates that the angular velocities are in the same direction, consequently, they form a ferromagnetic state. Notice that $|\omega_l| \approx |\omega_r|$ as in the antiferromagnetic state. In Fig. 3(b), we show a typical velocity field for this state. Here, both vortices exhibit significant overlap contrasting with the antiferromagnetic state, making it difficult to distinguish to which vortex a particle belongs; therefore, when associating particles with a particular vortex, we consider them belonging to the vortex to which they are closer. There is a third possible outcome for the correlation function, which we omit here, since it does not occur frequently, namely the uncorrelated state, $C_{\omega_l\omega_r} \approx 0$. We observe that although the vortices may be in either of the correlated states in a single run, they rarely change rotation directions. This pattern is usually observed when the vortices are widely separated, as we will show below. Finally, we

also observe an uncorrelated state on the boundary between the two correlated phases, and in this case, usually only one vortex is present.

In previous works [8, 11], it was shown that the rotation of a single vortex mainly depends on the obstacle diameter. We state that, for two obstacles, their distance (gap), as well as the particle density, can also be an important factor that determine correlations. Therefore, we present the results of the dependence of the correlation function on the gap, obstacle diameter, and particle density.

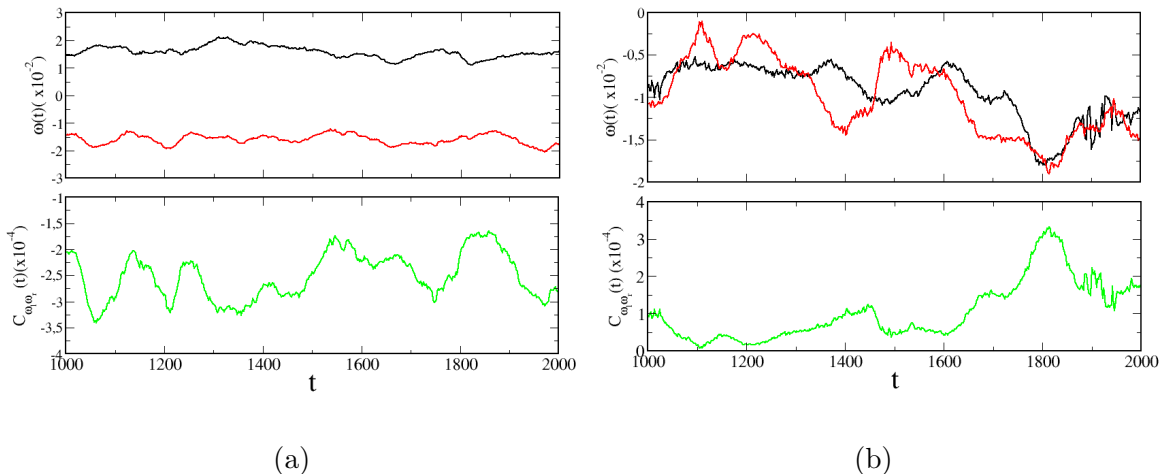


FIG. 2: The time dependence of the angular velocities of the left vortex (ω_l), black curves, and the right vortex (ω_r), red curves, along with the corresponding mean correlation function over essay (lower panels) for (a) the antiferromagnetic state at $\delta = 10$, $D = 40$, $\phi = 0.25$, and (b) the ferromagnetic state at $\delta = 2$, $D = 25$, $\phi = 0.30$.

The velocity fields shown in Figs. 3(a) and (b) give us an indication of the shape of the vortices in these correlated states. For the antiferromagnetic state, Fig. 3(a), we observe that both vortices are well separated and exhibit the typical isolated rotation pattern around each corresponding obstacle. However, they overlap in the inner region between them, where the particle current is strong and comparable to the vortex mean tangential velocity. On the other hand, in the ferromagnetic state, Fig. 3(b), the vortices rotate around both obstacles as a single structure, with the inner current lower than the mean tangential velocity. Given these patterns of motion, we refer to them as cog-like correlation [*cf.* Fig. 3(c)] for the antiferromagnetic case, and belt-like correlation [*cf.* Fig. 3(d)] for the ferromagnetic case. See videos of both states in the supplemental material. Both motion patterns were reported in ref [16] for bacteria in a square lattice of interconnected chambers. In this

experiment, the transition between regimes was achieved by increasing the width of the channels that connected neighboring chambers, and is a consequence of the underlying fluid currents induced by the bacteria, as in a typical wet model context. Below, we will see how this transition is achieved in our dry model.

In Fig. 4, we show the correlation function as a function of the diameter of the obstacles (D) for different δ and ϕ . For the smallest gap $\delta = 2$, Fig. 4(a), we observe a predominance of ferromagnetic regime for any ϕ , with a decreasing $C_{\omega_l\omega_r}$ as D increases, eventually reaching nearly zero correlation for $\phi = 0.20$ and $D = 40$. We also see that for $D \leq 25$, the correlation is smaller for larger ϕ , while, for $D > 25$, this behavior is inverted. At $\delta = 4$, Fig. 4(b), we observe the reduction of the intensity of positive correlation and the emergence of the antiferromagnetic regime, $C_{\omega_l\omega_r} < 0$ as compared to the $\delta = 2$ case, mainly for $\phi = 0.20$ and $D \geq 30$, while for larger ϕ , it appears only for $D = 40$. Finally, contrary to the earlier behavior with ϕ , increasing density results in an overall increase of correlation at fixed D .

In Fig. 4(c), we show the results for $\delta = 10$. We observe both correlated states, but now the antiferromagnetic state is more prominent compared to the ferromagnetic one, in agreement with the behavior change observed when we passed from the $\delta = 2$ to the $\delta = 4$ cases. For $\phi = 0.20$, the correlation is negative for any D , while for $\phi > 0.20$, this regime occurs only for $D \geq 30$. For smaller obstacles, we still observe a positive, although small, correlation. Finally, in Fig. 4(d), we present the results for $\delta = 20$; we see that the antiferromagnetic state occurs in almost all cases; also, we see that the correlation function value has a weaker dependence on ϕ compared to the previous $\delta < 20$ results.

From the previous data, we observe that increasing the gap generally changes the correlated state from ferromagnetic (positive correlation) to antiferromagnetic state (negative correlation), while keeping D and ϕ constant. We can describe such scenario through the belt and cog analogies we described earlier. Let us consider initially the ferromagnetic state, such as the depicted in Fig. 3(b). We see that as we increase the gap, at fixed D and ϕ , the belt necessarily stretches, *i.e.*, the particles should travel a longer distance enclosing both obstacles. Then, if we continue this process, it will reach a snapping point, in which the particles will no longer be able to move around both obstacles, and we reach the transition region. The approach to this region is continuous, since the correlation function decreases with increasing gap. Hence, stretching the belt, necessarily decreases the correlation. By increasing this parameter even further, they will form isolated vortices, as seen in Fig. 3(a).

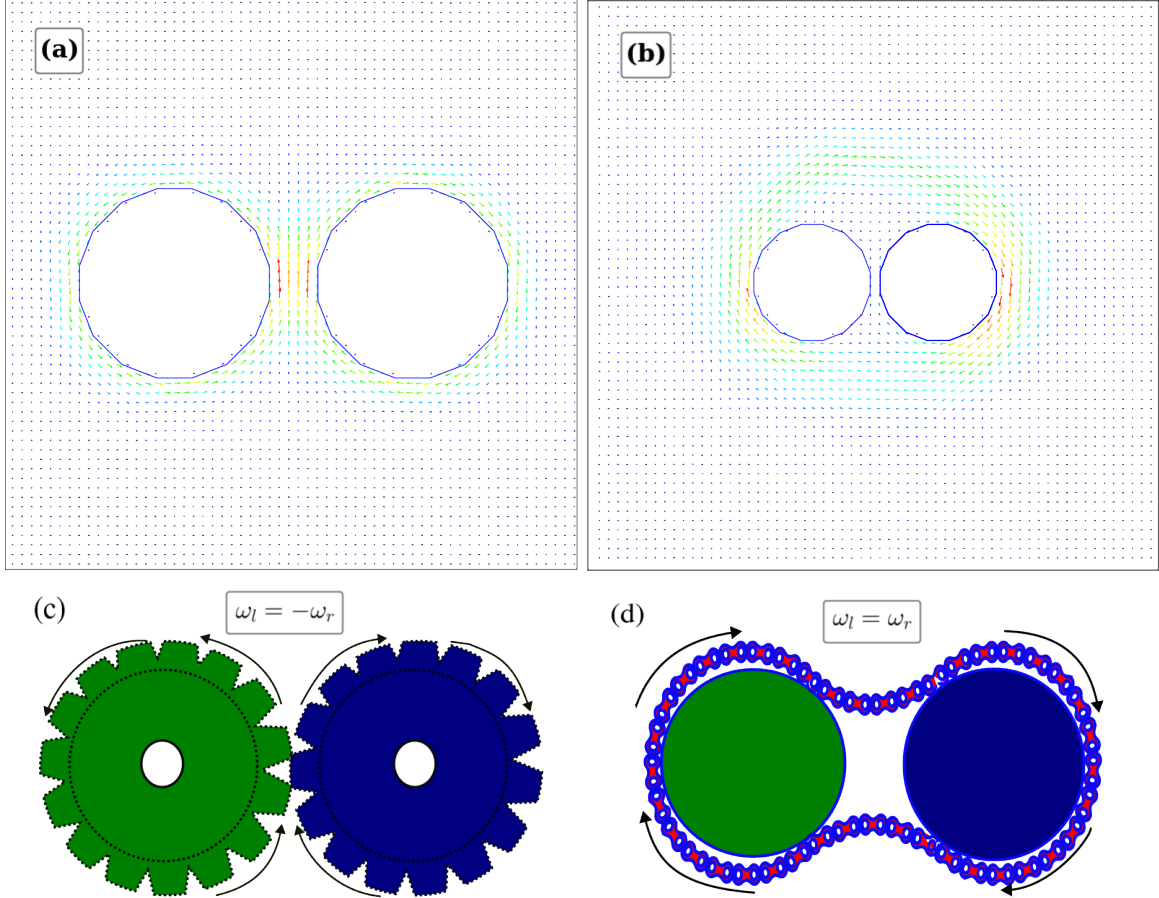


FIG. 3: Mean velocity field: (a) for $\phi = 0.25$, $\delta = 10$ and $D = 40$; (b) $\phi = 0.30$, $\delta = 2$ and $D = 25$. Illustrations of the (c) cog correlation, and (d) belt correlation.

At this point, the antiferromagnetic pattern arises as the correlated state. We present the dependence of $C_{\omega_l \omega_r}$ with δ for different D and ϕ in Fig. 5.

We see that the decrease of the correlation intensity with increasing δ is seen more clearly here, especially for $\delta \leq 8$, for any D . However, for larger gaps, the behavior is rather noisy, and more difficult to determine. We believe that, for lower gaps, since the obstacles are closer, they exchange more particles and, as a consequence, the correlated states are more evident. This raises the question of whether the vortices, whose correlations are negative as see in Figs. 4 (d) and Fig. 5, are really correlated, or only slightly perturbed by the presence of the other vortex. This is markedly important for larger obstacles $D \geq 35$, since we expect them to be in the stable vortex state, meaning that they rarely change their rotation directions throughout the simulation. We will address this issue below.

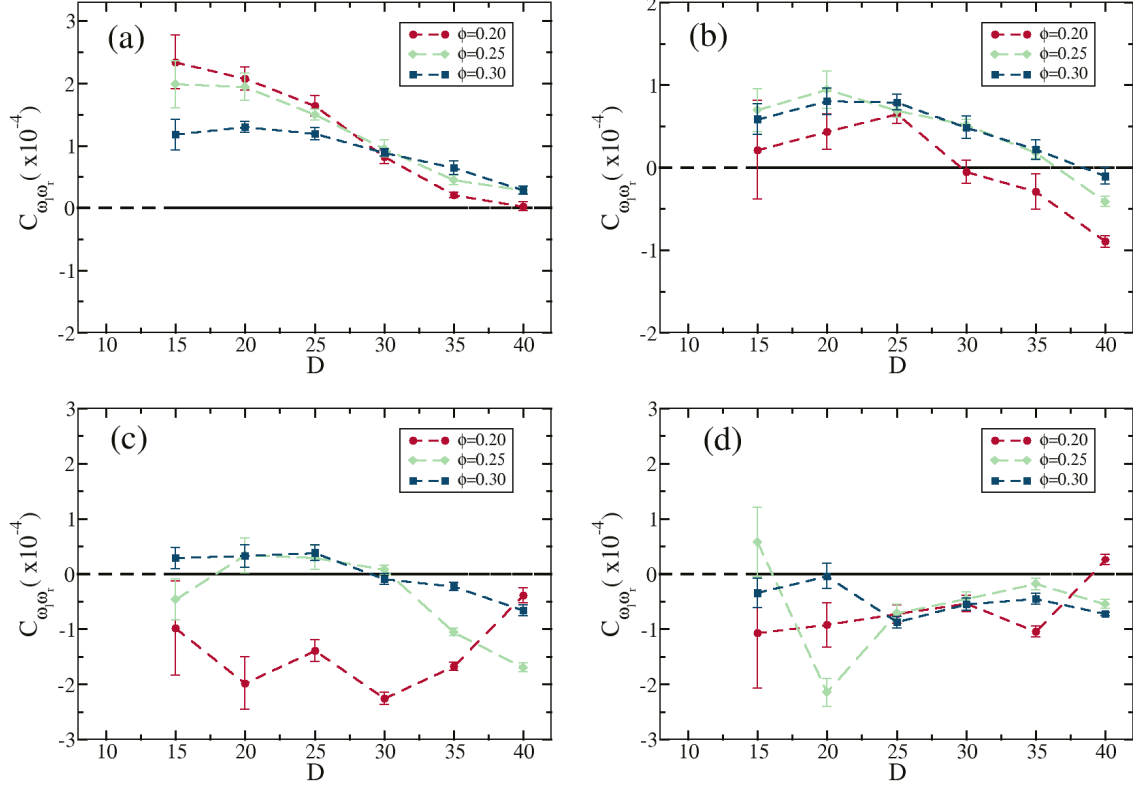


FIG. 4: Correlation function (C_{ω_l, ω_r}) as a function of obstacle diameter (D), for different ϕ for: (a) $\delta = 2$; (b) $\delta = 4$; (c) $\delta = 10$ and (d) $\delta = 20$.

In general, as aforementioned, the correlation tends to decrease with increasing δ , mainly for $\phi = 0.30$, Fig. 5(c). Based on the observation that active particles tend to stick to solid surfaces, increasing ϕ results in more particles captured by vortices [8, 11], making them more dense and robust. In terms of the belt and cog patterns, we may say that for more dense systems, the belts and cogs will be "thicker", meaning that a larger gap is required to reach the belt snapping point or the lowest correlation point as compared to those at lower ϕ . We also have data for $\phi < 0.20$ and $\phi > 0.30$, that show that the correlations are lost in these regimes since, in the former, the vortices have too few particles to produce any correlated state; in the latter, a dense structure is formed around both obstacles that prevents any rotation. In other words, in both cases, there are no observable rotating vortices.

Finally, regarding the dependence of the correlation on the obstacles' diameter, we observe a general decrease of the correlation with increasing D , but this tendency is clearer for $\phi = 0.30$, see Fig. 5(c). For the other two density values, the δ range in which we see this tendency is shorter for lower ϕ , for instance, for $\phi = 0.20$ the correlation function decreases

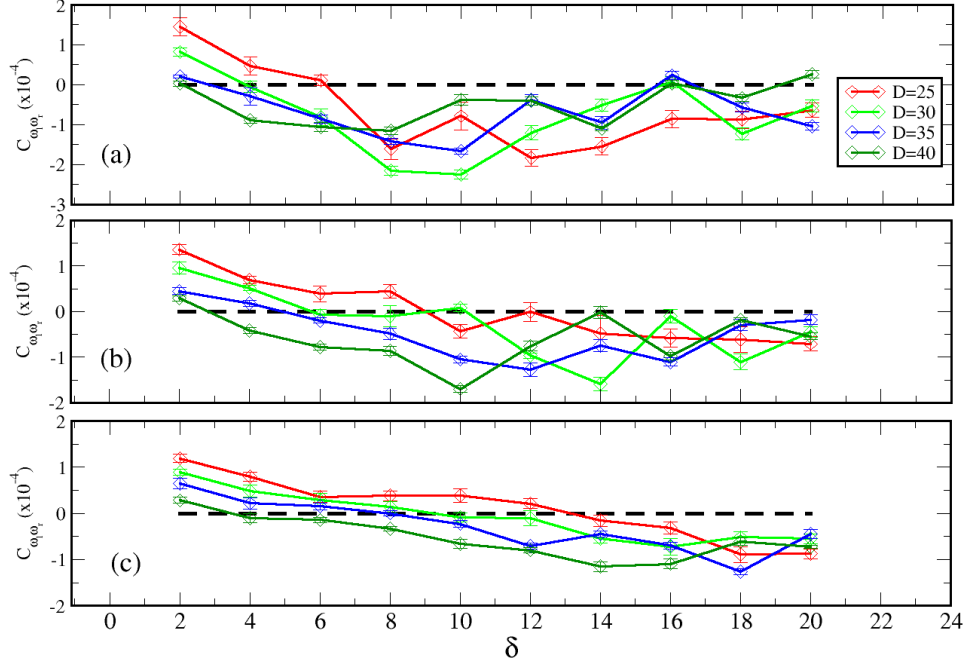


FIG. 5: Correlation function $C_{\omega_l \omega_r}$ as a function of gap δ for distinct obstacle's diameter D , for particle density (a) $\phi = 0.20$; (b) $\phi = 0.25$; and (c) $\phi = 0.30$.

with D clearly only up to $\delta \leq 6$, while for $\phi = 0.25$, only up to $\delta \leq 8$. We also see that, after the point of lowest correlation (which occurs at larger δ for larger ϕ), the dependence on D is more difficult to determine, since the data is rather noisy in this large gap regime, although this noise is smaller for larger ϕ . Again, the belt and cog analogies are helpful in interpreting these results. In the ferromagnetic regime, as we increase the obstacles' diameter, the particles should run a longer path in order to circumvent both obstacles, effectively stretching the belt. Therefore, increasing D , at fixed ϕ and δ , would naturally decrease the correlation, as stated above. In the antiferromagnetic regime, a similar effect takes place: for larger obstacles, the correlation decrease, at constant density, because the vortices would have less particles, since the surface they stick to are larger, resulting in smaller cogs that would reach out to each other for the correlation to occur.

Now, we comment on the large gap regime, $\delta \geq 10$. We see from our results, Figs. 4 and 5, that the results suggest either an antiferromagnetic state, or uncorrelated states. These features are observed for any D and ϕ . We state that some of these states are actually uncorrelated, but we hardly obtain $C_{\omega_l \omega_r} \approx 0$. In any simulation, due to the possibility of vortices rotating in the same or in the opposite directions, the correlation function will

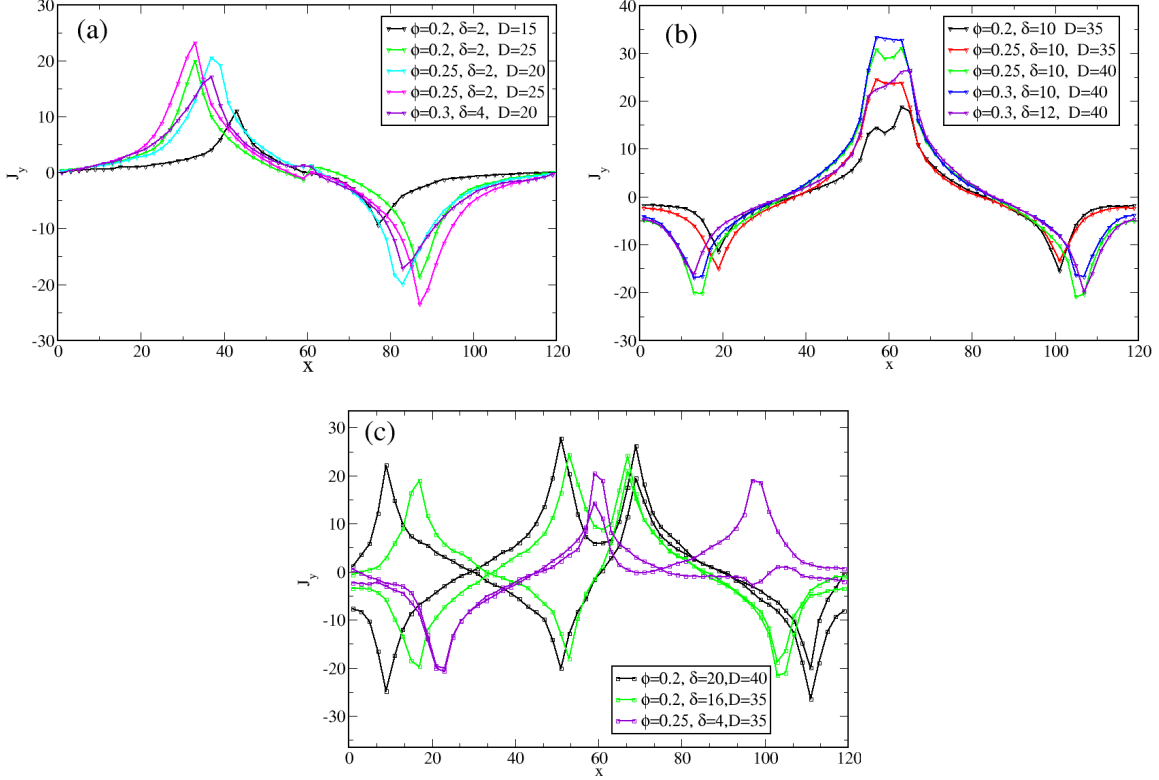


FIG. 6: Mean vertical particle current profiles as a function of the horizontal position x for (a) ferromagnetic and (b) antiferromagnetic states. In (c), we show a single run profiles for three uncorrelated states.

eventually exhibit a non-zero result, even for $D = 25$, which is not in the stable vortex regime [8]; hence, unless the simulation is very long, or there is a large number of independent runs, we are unable to improve statistical accuracy and obtain a vanishing correlation function. As a consequence, the distinction between a correlated and an uncorrelated state is not easily seen from the correlation function data. Nevertheless, we can distinguish uncorrelated states by the general shapes of the vertical velocity horizontal profiles, $J_y(x)$ (in fact, this provides an easier method to observe this distinction compared to the observations of the velocity fields, but both data sets yield the same results). We see that each state has a particular signature for this profile.

In Figs. 6(a) and (b), we show the mean vertical velocity horizontal profiles measured directly from the velocity fields. We see that the ferromagnetic states, Fig. 6(a), exhibit two peaks of nearly the same magnitude but of contrary signs, and occurring nearly at the outermost vertical tangent of the obstacles, *i.e.*, at $x_{l,r} = L/2 \mp (D + \delta/2)$, the plus(minus)

sign refers to the right(left) obstacle. Specifically, the peaks occur at the leftmost point of the left obstacle and at the rightmost point of the right obstacle, which indicates a single rotating structure, or a belt around both obstacles, since at the center of the system, $x = L/2$, the current changes sign, indicating that the vortices have opposite tangential velocities at that location, and is close to zero. For the antiferromagnetic states, see Fig. 6(b), there are three peaks: two occur, again, at $x_{l,r}$, and are nearly of the same magnitude and have the same sign, and a third peak situated at the center of the system. This third peak is broader than the others, spanning the entire gap, with a distinct sign compared to the other peaks and larger in magnitude. This indicates the presence of a strong particle current in the space between the vortices, stronger than the tangential velocities of the isolated vortices, as aforementioned, which is formed by particles in both vortices that travel in the same direction in that region. Finally, for the uncorrelated states, Fig. 6(c), there are four peaks, see the black and green curves for this behavior at two distinct parameter sets, two for each obstacle. They are nearly equal resulting in a positive correlation, or are reflected at the center of the system resulting in a negative correlation. In both cases, the particle current at the center is lower than the peak of the tangential velocities at the vortices. Finally, there is a third possibility for the vertical current profile in an uncorrelated state, seen in the purple curves in Fig. 6(c): here, one of the vortices (specifically, the right one) is not fully formed. This is seen when the profile, crossing the center of the box, exhibits a single peak, which is not characteristic of a rotating vortex, or is nearly flat, typical of an absent vortex. This corresponds to the belt-snapping point we mentioned earlier; it is a state transitioning from a ferro- to an antiferromagnetic state and marks the phase boundary between them.

By analyzing all profiles for the cases studied, we generated in Fig. 7 a set of δ vs. D phase diagrams for different ϕ indicating the observed correlations. Given the variability of the profiles, we defined two parameters for the identification of the correlated states. After determining that the state is antiferromagnetic, by observing the shape of the vertical particle current profiles for each run, we calculate the following ratio

$$\mathcal{A} = \frac{2|J_y(L/2)|}{|J_y(x_l)| + |J_y(x_r)|},$$

which is the one between the vertical velocity at the center of the system to the mean vertical velocity at $x_{l,r}$ for each run. If the mean value of this ratio over all runs is larger than 0.5, we consider this state to be an antiferromagnetic one. On the other hand, if we observe

that the system is in the ferromagnetic state, again, by observing the shape of the vertical velocity profiles, we calculate the ratio

$$\mathcal{F} = \frac{|J_y(x_l) + J_y(x_l + D)| + |J_y(x_r) + J_y(x_r - D)|}{|J_y(x_l)| + |J_y(x_r)|},$$

which is the one between the sum of the vertical velocities of a vortex at the outermost and the innermost vertical tangent, for both vortices to the sum of the vertical velocities at $x_{l,r}$. In this case, if the mean value of \mathcal{F} over all runs is also larger than 0.5, the system is considered to be in the ferromagnetic state. These criteria are chosen so that the resulting phase diagrams reflect the data show in Figs. 4 and 5 for the correlation function. In all other cases, we consider the system to be uncorrelated. Notice, in Fig. 7, that the antiferromagnetic state is more common than the ferromagnetic one. Also, we see that the ferromagnetic state occurs for a wide δ range at $D = 25$, suggesting that the belt is more easily formed for smaller obstacles. Additionally, increasing density enlarges the parameter range in which both states appear, while decreases the parameter range of the uncorrelated states in agreement with the analogy of thicker belts and cogs stated earlier.

IV. CONCLUSIONS

We investigated the dynamics of dry active matter in the presence of two identical circular obstacles and focused in the correlations between the rotations of the vortices formed around each obstacle. We carried out simulations as a function of the obstacle size D , obstacle separation (gap) δ , and particle density ϕ . We observed two distinct regime regarding the vortices' motion around the obstacles: ferromagnetic, characterized by a positive correlation, or co-rotating vortices; and antiferromagnetic, characterized by a negative correlation, or counter-rotating vortices. The former is characterized by the merging of the two vortices in a single rotating cluster around both obstacles, resembling a belt strapped around them. This regime is primarily observed for low gap and obstacle size. The antiferromagnetic state, on the other hand, has both vortices occurring independently, but exchange a significant amount of particles in the region in between them, resulting in a non-vanishing vertical particle current at the center of system. This behavior resembles two synchronized cogs, and it is typically observed for intermediate gap and large obstacle size. In either case, we can say that the vortices motions are synchronized in a belt-like pattern or in a cog-like

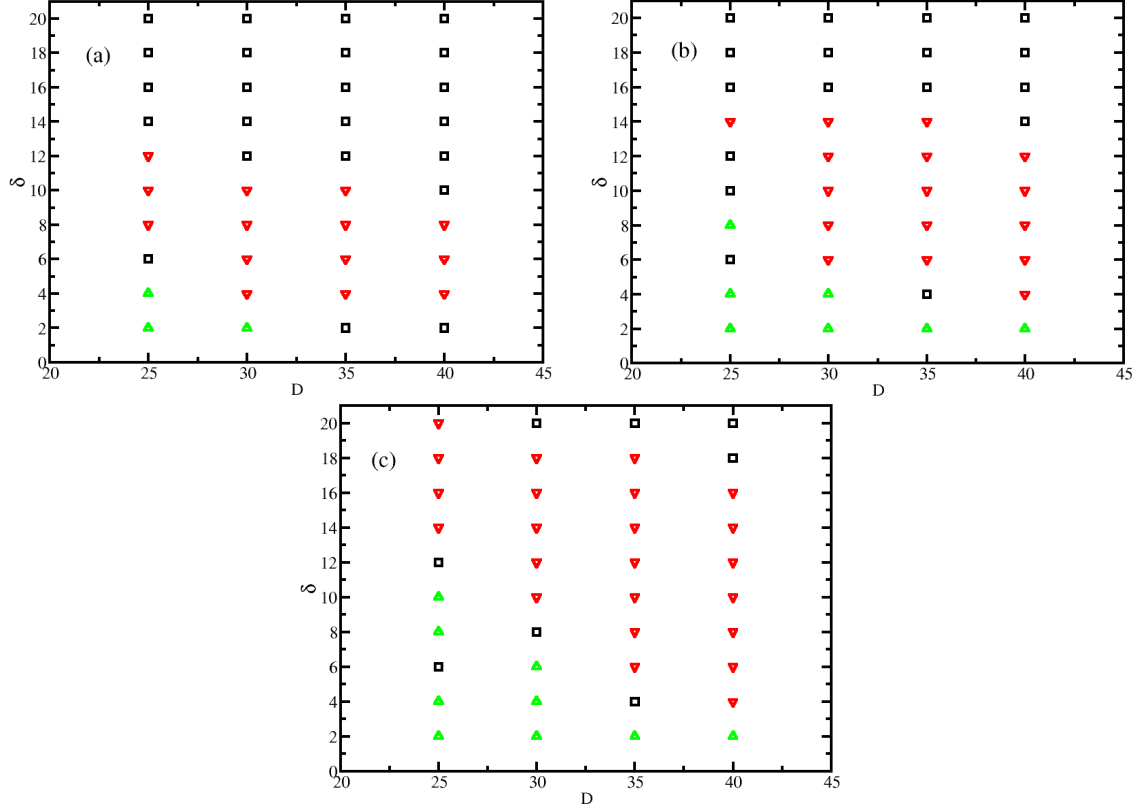


FIG. 7: Phase diagrams δ vs. D for $D \geq 25$ at (a) $\phi = 0.20$; (b) $\phi = 0.25$; and (c) $\phi = 0.30$.

Red inverted triangles represent antiferromagnetic states, black squares, uncorrelated states, and green triangles, ferromagnetic states.

pattern.

We also observed the occurrence of uncorrelated states in which, although the correlation function does not vanish (which would indicate such a state), the particles moving around the obstacles do not match either of the two synchronized states. In this case, the vortices are isolated, with no discernible overlap between them, and can be either in a ferro- or in an antiferromagnetic state. In the ferromagnetic state, the vertical-central particle current vanishes with no belt of particles around both obstacles, while in the antiferromagnetic state, there is a non-zero vertical-central particle current, but it is smaller than the vortices' tangential velocity. The uncorrelated state occurs mainly for intermediate to large gap values, and for large obstacle sizes. We also observed uncorrelated states in which only one vortex is present; this corresponds to the belt snapping point and marks the transition between the two correlation regimes.

Finally, the effect of varying density in this scenario is to strengthen the correlation. That

is, when we increase the particle density, the ranges of δ and D in which both correlated states occur become larger. We interpreted this result as a strengthening of the vortices: they capture more particles allowing the obstacles to be placed farther apart or to be larger, while still exhibiting one of the two correlated motion states.

A possible future direction for this investigation is the extension of the current setup to a regular lattice of circular obstacles in order to explore whether any synchronized state, similar to those observed for wet models [16, 19], emerges. This is actually a challenging problem because achieving an uniform distribution of particles throughout the lattice is rather difficult, given the clustering tendency observed in dry active matter. Alternatively, we may observe pairs of correlated vortices in a lattice of obstacles, but their behavior would likely resemble what we have just described.

V. ACKNOWLEDGEMENTS

The authors acknowledge financial support from CAPES, CNPq, FAPESPA, and FUNCAP.

-
- [1] M. C. Marchetti, J. Joanny , S. Ramaswamy, T. Liverpool *et al.*, *Rev. Mod. Phys.* **85**, 1143 (2013).
 - [2] H. Ribeiro, W. P. Ferreira, and F. Q. Potiguar, *Phys. Rev. E* **101**, 032126 (2020).
 - [3] M. Das, C. Schmidt, and M. Murrell, *Soft Matter* **16**, 7185-7190 (2020).
 - [4] M. Cates, D. Marenduzzo, I. Pagonabarraga, and J. Tailleur, *Proc. Nat. Acad. Sci.* **107**, 11715-11720 (2010).
 - [5] T. Vicsek, A. Czirók, E. Ben-Jacob, I. Cohen and O. Shochet , *Phys. Rev. Lett.* **75**, 1226 (1995).
 - [6] Y. Fily, and M. C. Marchetti, *Phys. Rev. Lett.* **108**, 235702 (2012).
 - [7] M. Cates, and J. Tailleur, *Europhys. Lett.* **101**, 20010 (2013).
 - [8] J. Pan, H. Wei, M. Qi, H. Wang, *et al.*, *Soft Matter* **16**, 5545-5551 (2020).
 - [9] Y. Fily, A. Baskaran, and M. Hagan, *Soft Matter* **10**, 5609-5617 (2014).
 - [10] S. Spagnolie, G. Moreno-Flores, D. Bartolo, *et al.*, *Soft Matter* **11**, 3396-3411 (2015).

- [11] Z. Mokhtari, T. Aspelmeier, and A. Zippelius, *Europhys. Lett.* **120**, 14001 (2017).
- [12] D. Takagi, J. Palacci, A. Braunschweig *et al.* , *Soft Matter* **10**, 1784-1789 (2014).
- [13] B. Qian, K. Chen *et al.* , *Phys. Chem. Chem. Phys.* **23**, 20388-20397 (2021).
- [14] G. Volpe, I. Buttinoni, D. Vogt *et al.* , *Soft Matter* **7**, 8810-8815 (2011).
- [15] F. Q. Potiguar, G. Farias, and W. P. Ferreira, *Phys. Rev. E* **90**, 012307 (2014).
- [16] H. Wioland, F. Woodhouse, J. Dunkel, and R. Goldstein, *Nat. Phys.* **12**, 341-345 (2016).
- [17] K. Beppu, Z. Izri, J. Gohya, and others, *Soft Matter* **13**, 5038-5043 (2017).
- [18] H. Reinken, S. Klapp, M. Bär, and S. Heidenreich, *Phys. Rev. E* **97**, 022613 (2018).
- [19] H. Reinken, S. Heidenreich, M. Bär, and S. Klapp, *Phys. Rev. Lett.* **128**, 048004 (2022).
- [20] K. Gowrishankar, and M. Rao, *Soft Matter* **12**, 2040 (2016).
- [21] N. Rana, and P. Perlekar, *Phys. Rev. E* **102**, 032617 (2020).
- [22] N. Rana, and P. Perlekar, *Phys. Rev. E* **105**, L032603 (2022).
- [23] J. Toner, and Y. Tu, *Phys. Rev. Lett.* **75**, 4326 (1995).
- [24] M. Marchetti, Y. Fily, S. Henkes, and others, *Curr. Opin. Colloid Interface Sci.* **21** pp. 34-43 (2016).
- [25] D. Rapaport, The art of molecular dynamics simulation. (Cambridge university press,2004)
- [26] A. Borba, Jorge L. C. Domingos, E. Moraes, F. Q. Potiguar, and W. P. Ferreira, *Phys. Rev. E* **101**, 022601 (2020).